

Real-time observations of the transition dynamics between multiple nonlinear states in a coherently driven Kerr fiber-loop resonator

Yayu Cao(曹亚昱), Heng Dong(董恒), and Xiankun Yao(姚献坤)
Citation: Chin. Phys. B, 2025, 34 (**7**): 074206. DOI: 10.1088/1674-1056/adc40a
http://cpb.iphy.ac.cn; http://iopscience.iop.org/cpb

What follows is a list of articles you may be interested in

Controlled propagation and particle manipulation of off-axis-rotating elliptical Gaussian beams in strong nonlocal media

Rong-Quan Chen(陈荣泉), Rui-Lin Xiao(肖瑞林), Wei Wang(王伟), Xi-Xi Chu(储茜茜), Yu-Qing Song(宋雨晴), Xu-Dong Hu(胡旭东), and Ming Chen(陈明)
Chin. Phys. B, 2025, 34 (**3**): 034205. DOI: 10.1088/1674-1056/ada9dd

Passive on-chip isolators based on the thin-film lithium niobate platform

Jiacheng Liu(刘嘉成), Gongyu Xia(夏功榆), Qilin Hong(洪琦琳), Pingyu Zhu(朱枰谕), Kai-Kai Zhang(张凯凯), Keyu Xia(夏可宇), Ping Xu(徐平), Shiqiao Qin(秦石乔), and Zhihong Zhu (朱志宏)
Chin. Phys. B, 2025, 34 (**3**): 034204. DOI: 10.1088/1674-1056/ada2ef

Four-wave mixing Bragg scattering for small frequency shift from silicon coupled microrings

Chang Zhao(赵畅), Chao Wu(吴超), Pingyu Zhu(朱枰谕), Yuxing Du(杜昱星), Yan Wang(王焱), Miaomiao Yu(余苗苗), Kaikai Zhang(张凯凯), and Ping Xu(徐平)
Chin. Phys. B, 2025, 34 (**1**): 014206. DOI: 10.1088/1674-1056/ad8a4f

Manganese dioxide as wide adaptive ultrafast photonic device for pulsed laser generation

Xin-He Dou(窦鑫河), Zhen Chen(陈震), Chen-Yan Zhang(张辰妍), Xiang Li(李响), Fei-Hong Qiao(乔飞鸿), Bo-Le Song(宋博乐), Shan Wang(王珊), Hao Teng(滕浩), and Zhi-Guo Lv(吕志国)
Chin. Phys. B, 2024, 33 (**11**): 114202. DOI: 10.1088/1674-1056/ad71b5

Plasmon-induced nonlinear response on gold nanoclusters

Yuhui Song(宋玉慧), Yifei Cao(曹逸飞), Sichen Huang(黄思晨), Kaichao Li(李凯超), Ruhai Du(杜如海), Lei Yan(严蕾), Zhengkun Fu(付正坤), and Zhenglong Zhang(张正龙)
Chin. Phys. B, 2024, 33 (**4**): 044204. DOI: 10.1088/1674-1056/ad1a8b

---

Real-time observations of the transition dynamics between multiple nonlinear states in a coherently driven Kerr fiber-loop resonator

Yayu Cao(曹亚昱)[1], Heng Dong(董恒)[1], and Xiankun Yao(姚献坤)[1,2,3,†]

[1] *School of Physics, Northwest University, Xi'an* 710127, *China*
[2] *Shaanxi Key Laboratory for Theoretical Physics Frontiers, Xi'an* 710127, *China*
[3] *Peng Huanwu Center for Fundamental Theory, Xi'an* 710127, *China*

(Received 18 February 2025; revised manuscript received 13 March 2025; accepted manuscript online 24 March 2025)

Passive Kerr fiber-loop resonators driven by coherent lasers exhibit a variety of nonlinear states, including modulation instability (MI), localized dissipative structures (solitons), and chaos. Although these transitions have been predicted theoretically, experimental real-time observations are rare in coherently driven Kerr fiber-loop resonators. In this study, we observed real-time transitions between the predicted nonlinear states by sweeping detuning both positively and negatively. We discovered the transition path between nonlinear states depending on the direction of detuning, providing new insights into the nonlinear dynamics. Our findings directly validate theoretical predictions and offer potential implications for future nonlinear optical applications.

Keywords: nonlinear optics, cavity solitons, Kerr resonator, modulation instability

PACS: 42.65.Tg, 42.81.Dp, 42.65.Sf, 42.65.–k

DOI: 10.1088/1674-1056/adc40a **CSTR:** 32038.14.CPB.adc40a

1. Introduction

As the simplest nonlinear optical cavity, Kerr fiber-loop resonators capture the main dynamical features and have played a crucial role in the study of complex cavity dynamics,[1–6] particularly in localized dissipative structures[3,7–11] (cavity solitons, CSs) in nonlinear non-Hermitian systems. In Kerr cavities, the combined effects of nonlinearity and dispersion result in rich physical phenomena,[4,7,12–17] notably modulation instability (MI), and cavity soliton (CS) formation.[3,10,18–21] The Lugiato–Lefever equation (LLE) is typically used to describe nonlinear behavior within Kerr fiber-loop resonators.[10,22–25] As a standard pattern formation equation, the LLE is widely applied to non-equilibrium systems and provides a standard description of coherent Kerr nonlinear cavities.[26] The steady-state solution of the LLE includes a dissipative Kerr CS.[1,24] Besides stable CSs, theoretical analysis reveals some dynamical instabilities,[24] such as breathing Turing patterns and breathing CSs.[27,28]

MI is common in conservative and dissipative physical systems[23,29,30] and is characterized by periodic perturbations on a strong continuous wave (CW) laser beam that grows and evolves exponentially. The MI is one of the most important processes in nonlinear science and is closely related to the formation of patterns, CSs,[31] and rogue waves.[32–34] The pulse sequences in the MI process are ideal CS sequences, which has led to the study of CSs. In Kerr fiber-loop resonators, MI leads to the emergence of stable periodic (Turing pattern) modes, which are closely related to spatiotemporal CSs and microresonator frequency combs.[2,8,35–38] Temporal CSs are typically interpreted as local excitations in the coexistence of periodic modes and a uniform background, connecting one period of the mode to a uniform background. Their existence is due to a balance of effects: the dispersive effect caused by group velocity dispersion is suppressed by the nonlinear effect of the material, and the energy loss during propagation in the cavity is compensated by the coherent driving beam. To date, only stable CSs[3,9,39–42] and periodically oscillating CSs[25,43] have been studied experimentally in coherently driven Kerr fiber-loop resonator. Considerable advances have been achieved in microresonator, where the dynamical processes of cavity soliton formation have been experimentally observed.[44–46] However, in coherent Kerr fiber-loop resonator, despite theoretical predictions, there is still a lack of direct experimental evidence for the complete and continuous transitions between multiple nonlinear states.

In this work, we report the complete real-time observation of the transition dynamics between multiple nonlinear states in a coherently driven Kerr fiber-loop resonator. By sweeping the pump detuning, we experimentally demonstrate the continuous transitions among four nonlinear states: stable MI, unstable MI, unstable CSs, and stable CSs. Notably, we discovered that the transition path between nonlinear states depends on the direction of detuning. Furthermore, during decreasing detuning, we observed a transition from stable CSs to stable MI, bypassing the anticipated breathing CSs. Our experimental re-

†Corresponding author. E-mail: yaoxk@nwu.edu.cn

© 2025 Chinese Physical Society and IOP Publishing Ltd. All rights, including for text and data mining, AI training, and similar technologies, are reserved.

sults, supported by numerical simulations based on the LLE, directly validate the theoretical predictions of multiple nonlinear states transitions in a detuning-varying coherently driven Kerr fiber ring cavity.

2. Numerical simulation

First, we describe the nonlinear dynamics that support our experiment. To do this, we used LLE to describe the dynamics of the coherently driven Kerr cavity. Its dimensionless[10,47–49] form is expressed as follows:

$$\frac{\partial U}{\partial t} = \mathrm{i}\frac{1}{2}\frac{\partial^2 U}{\partial \tau^2} + \mathrm{i}\,|U|^2 U + S - (\mathrm{i}\Delta + 1)\,U. \tag{1}$$

In a coherently driven Kerr cavity, U denotes the slowly varying envelope of the electric field, where τ is the fast time used to describe the temporal profile of the optical field and t refers to the slow time, which is used to describe the propagation time of the optical field along the cavity. It accounts for the evolution of the intracavity field over multiple round trips in the Kerr fiber-loop resonator or fiber ring cavity. The terms on the right-hand side of the equation represent the dispersion effect, nonlinear effect, pump term, detuning, and losses. Specifically, the normalization, $t = \alpha t/t_{\mathrm{R}}$, $\tau = \tau\sqrt{\alpha/|\beta_2|L}$, and $U = E(z,t)\sqrt{\gamma L/\alpha}$.

Here, t_{R} denotes the cavity round-trip time, β_2 (<0) is the group velocity dispersion coefficient, γ is the nonlinear coefficient, and α is half of the total power loss in the cavity. The normalized pump term is given by $S = E_{\mathrm{in}}\theta\sqrt{\gamma L/\alpha^3}$, where θ is the transmission coefficient of the pump field E_{in} into the fiber-loop resonator and L is the length of the fiber ring cavity. Finally, Δ represents the phase detuning between pump frequency ω and the nearest fiber-loop resonator eigenmode ω_0, $\Delta = \delta/\alpha$ and $\delta = (\omega_0 - \omega)t_{\mathrm{R}}$.

To illustrate the detuning intervals within which various nonlinear states can exist, we present the results in Fig. 1 through theoretical calculations and numerical simulations.[50] Figure 1(a) was acquired by means of the squared-operator iteration method and the Newton conjugate gradient method.[51] Among which, the blue line represents the peak power of MI (the blue solid line represents stable MI, and the blue dotted line represents unstable MI) and Δ_{MI} represents the lower limit for the existence of the stable MI mode, while the red solid line is indicative of stable CS and red dotted line signifies unstable CS. Black dashed part is unconditionally unstable, whereas the black solid and the dotted parts remain stable even under perturbations.

Notably, in Fig. 1(a), we identify a partial detuning interval where two nonlinear states coexist, a phenomenon previously predicted in the literature.[50] This result suggests that the nonlinear state transitions in the system exhibit path dependence, meaning that the transition trajectory can vary depending on the direction of detuning. This overlap can be attributed to bifurcation in the LLE, which play a key role in creating regions where multiple instabilities coexist. Under specific parameter ranges, the system can support either unstable MI or unstable CS. The final nonlinear state in the fiber ring cavity is primarily determined by system parameters, but the transition pathway leading to this state exhibits path dependence. In our numerical simulations, small perturbations were introduced to seed modulation instability, ensuring a physically realistic starting condition. As the system evolves, the direction of the detuning scan dictates which nonlinear states become accessible, revealing distinct transition pathways. Specifically, smaller detuning values tend to favor MI, while larger detuning promotes the formation of CSs. Additionally, higher pump power may expand the instability regions while enhancing the competition between MI and CS states. Figure 1(a) enables us to determine the detuning range in which each nonlinear state can exist. Figures 1(b)–1(e) illustrate these different behaviors from the direct numerical simulations of the LLE. These numerical simulations, performed at four representative fixed detuning values, employ system parameters identical to those in our experiments. Small perturbations were introduced to seed modulation instability, ensuring physically realistic conditions. The results shown in Figs. 1(b)–1(e) illustrate the typical nonlinear states theoretically expected at these specific detuning values and serve as clear theoretical references for understanding the path-dependent state transitions observed experimentally.

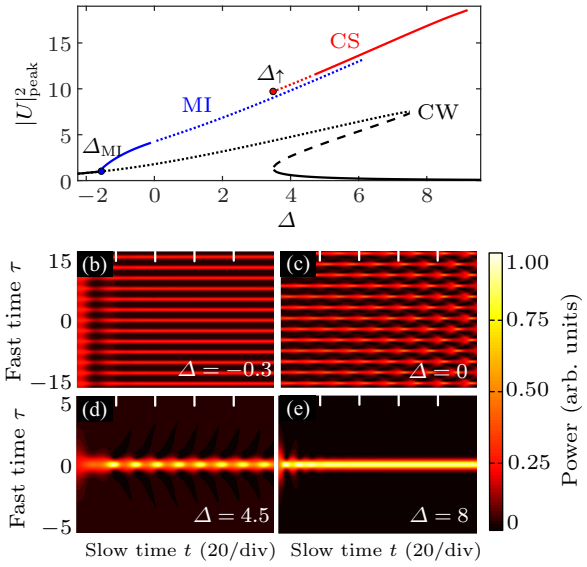


Fig. 1. Illustration of nonlinear structure examples: (a) black curve located at the bottom depicts the average power of the CW in the steady-state solution, while the blue curve represents the peak power of MI and the red curve at the top illustrates the peak power of CS under corresponding different detuning. (b)–(e) The numerical simulation dynamics under different conditions: (b) $\Delta = -0.3$, (c) $\Delta = 0$, (d) $\Delta = 4.5$, (e) $\Delta = 8$.

As shown in the dynamical evolution depicted in Fig. 1(b), under small detuning values, the MI remains stable, corresponding to the stable MI mode indicated by the blue solid line. When the detuning value increases to $\Delta = 0$, the

system transitions into the unstable MI region, characterized by the blue dotted line in Fig. 1(a), with the corresponding dynamics illustrated in Fig. 1(c). Further increasing the detuning to $\Delta = 4.5$ results in the emergence of a breathing CS. At this point, the system lies in the coexistence region of the stable MI mode and the unstable CS mode, as indicated by the overlap of the blue dashed line and the red dotted line in Fig. 1(a). The associated dynamical process is presented in Fig. 1(d). Finally, when the detuning reaches $\Delta = 8$, the system transitions into the stable CS. The CS evolution at this stage is shown in Fig. 1(e), corresponding to the red solid line in Fig. 1(a). For the CS solutions, the upper transition point $\Delta_{\uparrow}$ represents the lower limit for the presence of a CS. On the upper branch, the CS is stable at large detuning, but as the detuning decreases, the CS becomes unstable through a Hopf bifurcation (red dotted line).

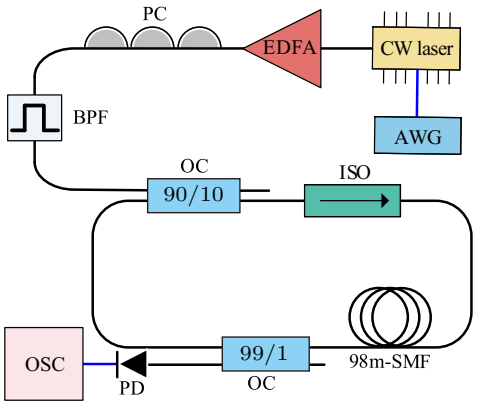


Fig. 2. Schematic diagram of the experimental setup. AWG: arbitrary waveform generator, EDFA: erbium doped fiber amplifier, PC: polarization controller, BPF: band-pass filter, ISO: isolator, PD: photodetector, OSC: oscilloscope, SMF: single-mode fiber.

3. Experimental setup

The experiment was performed using the setup[10] shown in Fig. 2. The fiber ring cavity is composed of a 98-meter-long single-mode fiber (SMF) ($\beta_2 \approx -21.4$ ps^2·km^{-1}; $\gamma \approx 1.3$ W^{-1}·km^{-1}; $\theta \approx \sqrt{0.1}$, $\alpha \approx 0.12$). The addition of a fiber isolator to the fiber ring cavity ensures the unidirectional transmission of light, preventing any reflected or backward-propagating light from re-entering the system. This is crucial for maintaining the stability of the intracavity optical field, as reflected light can interfere with the forward-propagating beam, causing instabilities or noise. To suppress the amplified spontaneous emission generated as the pump beam passed through the erbium-doped fiber amplifier, we placed a band-pass filter with a central wavelength of 1550.12 nm and bandwidth of 0.264 nm before it entered the 90/10 fiber coupler. The total finesse of the cavity was approximately 26 ($F \approx \pi/\alpha$), corresponding to a 24% loss of the beam for each round trip within the cavity. A 99/1 fiber coupler was used to monitor the dynamics within the cavity, and the output light was transmitted to an oscilloscope through a photodetector to observe the transitions between multiple nonlinear states in the time domain. It was closed using a 90/10 fiber coupler. The round-trip time of the cavity was approximately 475 ns, and the 76% power recirculation rate within the cavity effectively provided the Kerr nonlinearity effect.

To coherently drive the cavity, which allows the pump light to coherently add up during each round trip, the spectral width of the pump light must be narrower than the resonance width of the cavity. Therefore, we used a narrow-linewidth laser with a linewidth of 0.77 kHz and central wavelength of 1550.12 nm to generate the pump light and increase its power to 1.0 W using an erbium-doped fiber amplifier before the pump light entered the cavity.

To study the transition process between different nonlinear states, we used an arbitrary waveform generator to adjust the carrier frequency of the pump light at the pump laser, thereby systematically controlling detuning. As shown in Fig. 1(a), we started the experiment with blue detuning ($\Delta < 0$) and then continuously increased δ at a rate of $\mathrm{d}\delta/\mathrm{d}t = 2.68$ rad/ms. To directly observe the transition process of nonlinear states within the cavity, we utilized a real-time oscilloscope (Tektronix MSO73304DX) with a bandwidth of 33 GHz and sampling rate of 100 Gs sample/s (1 Gs = 10^{-4} T), the bandwidth of the photodiode is 50 GHz. This allowed us to observe the transition process of different nonlinear states as δ was varied.

4. Effects of increased detuning on intracavity dynamics

Figures 3(a) and 3(b) show the measured and simulated dynamics of the nonlinear state transition process, respectively. In the initial stage of the measurement, we observed an optical field that exhibited specific fluctuations. The measurement results were largely consistent with the theoretically predicted Hopf bifurcation, which occurs at a specific detuning value marking the transition of the light field from the MI state to the CSs, as shown in Fig. 1(a). To demonstrate the complete transition process between nonlinear states, we first set the system's initial state to an optical field characterized by specific fluctuations, prior to the emergence of the stable MI mode, that is, the black solid line in Fig. 1(a), with detuning below the MI threshold, $\Delta \approx -2$. Figure 3(a) shows the intracavity dynamics measured at the 99/1 coupler output.

MI occurs in the intracavity optical field when the pump power and detuning are in the proper range. For $\Delta = 1.5$, the CW split into periodic pulses, forming a stable MI. These pulses exhibited small fluctuations and strong periodicity. As the detuning further increases to $\Delta = 3$, the MI becomes unstable, leading to irregular periodic pulses and resulting in increased fluctuations in the pulse intensity. At this stage, the

MI is unstable, and the optical field displays chaotic dynamic behavior. As detuning continues to increase to $\Delta = 5$, the unstable MI transitions to the breathing CSs state. Breathing CS represents a distinct CS variety, serving as a particular transitional phase between entirely unstable CSs and stable CSs. It is marked by a periodic oscillation in both intensity and width over time, manifesting as a "breathing" behavior. Upon the detuning increasing continuously to $\Delta = 7.2$, the breathing CS ceases its breathing behavior and transits into a stable CS state, whereby the pulse intensity and width remain unaltered. Notably, owing to the chaotic nature of the dynamics, certain CSs persist in oscillating until they vanish. Stable CSs are distinguished by their invariant intensity and width, thereby generating and maintaining stable pulses within the cavity. This phenomenon indicates the terminal state of the nonlinear state transformation.

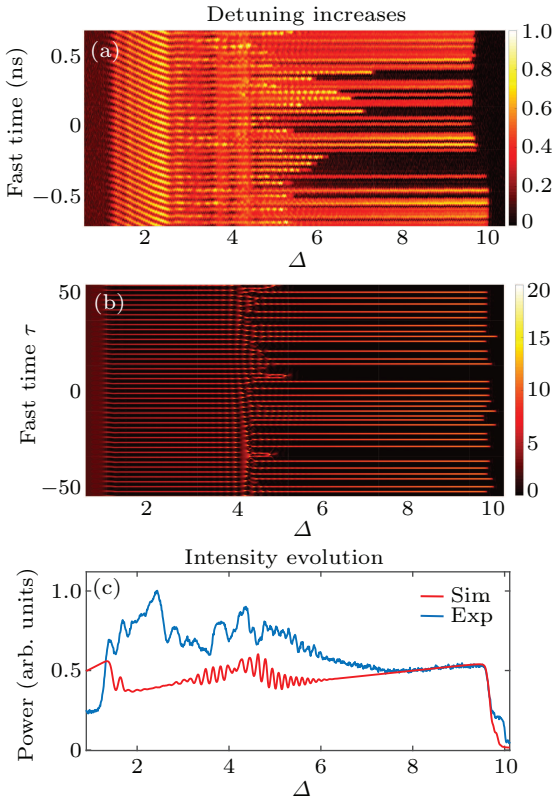


Fig. 3. (a) The 450-ns experimental measurements of the spatiotemporal evolution within the cavity as Δ continuously increases. (b) The numerical simulation results of the experiment shown in panel (a). (c) The relationship between the intracavity power and Δ.

It is worth noting that the experimental results shown in Fig. 3 show a significant "drift" of the stabilized MI, which is inconsistent with the numerical simulation results. We attribute the observed drift phenomenon to the electrostriction, induced by high intracavity power, which causes slight variations in the cavity length. These variations affect the repetition frequency, while the experimental data acquisition assumes a fixed repetition frequency. Figure 3 demonstrates that MI appears at a detuning value of 1.5, which is different from the theoretically predicted point -2 in Fig. 1(a). This discrepancy arises because the theoretical prediction is based on fixed detuning points, whereas our study employs dynamic scanning of the detuning process. Additionally, the formation of different nonlinear states requires a certain amount of time to evolve, leading to a delay in the observed transitions. This time-dependent evolution results in our experimental findings being somewhat different from the theoretical predictions, reflecting a "delay" phenomenon. Figure 3(c) depicts the relationship between intracavity power and detuning. The blue solid line corresponds to the experimentally measured average power, whereas the red line represents the numerically simulated average power. In the stable MI state, the intracavity mean power increases linearly with detuning, as the MI state dominates the cavity field. Upon entering the unstable MI state, enhanced local field fluctuations lead to power oscillations. As the system transitions into the CSs regime, the mean power decreases significantly, since CSs occupy localized regions of the cavity field, and the background field strength weakens. This behavior aligns with theoretical predictions and experimental observations reported in the literature,[40,41] confirming the dynamic transitions between MI and CS states. This relationship is an important basis for us to judge the nonlinear state in the cavity.

5. Effects of decreased detuning on intracavity dynamics

To explore the nonlinear transition process within the cavity as detuning gradually decreases, we conducted another experiment after CSs generation ($\Delta \approx 8$) using a slower detuning reduction rate ($\mathrm{d}\delta/\mathrm{d}t = -1.34$ rad/ms) and obtained satisfactory results. Figure 4(a) shows the signal captured by the oscilloscope when Δ decreased from $\Delta \approx 8$. We estimated that during the entire measurement process, Δ decreases from approximately 8 to -0.5. Under large detuning conditions, stable CSs form within the cavity, with the pulse intensity and width remaining constant, and the optical field is in a stable CS state. During decreasing detuning, the intracavity optical field undergoes a series of nonlinear state transitions, progressing from stable CS states to unstable MI states and ultimately reaching stable MI states.

In the initial stage, the optical field is in a highly localized stable CS state, with energy concentrated within the CS pulses and negligible energy distributed in the background field. As detuning decreases further, the localized nature of the CSs state breaks down, and the system transitions into the unstable MI region, characterized by spatially modulated patterns occupying a larger portion of the energy distribution. Upon further detuning reduction, the system eventually enters the stable MI state, where the optical field exhibits a uniformly distributed modulation structure, and intracavity modes become relatively stable. The corresponding numerical simulation is shown in

Fig. 4(b), where we observe that the dynamic process occurring within the cavity matches the results simulated by Eq. (1). A number of experimental observations have been carried out which are in good agreement with the numerical simulations.

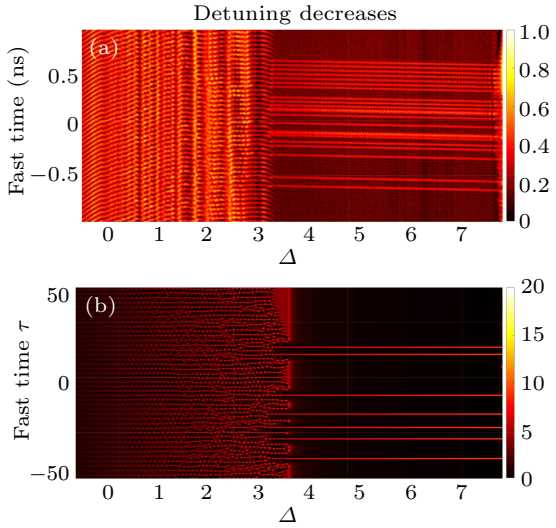


Fig. 4. (a) The experimental measurements of the spatiotemporal evolution within the cavity as Δ continuously decreases. (b) The numerical simulation results of the experiment.

To better understand the role of detuning direction in nonlinear state transitions, we compared the experimental results under increasing and decreasing detuning conditions. Under increasing detuning, the system undergoes a continuous transition from MI to CSs. By contrast, under decreasing detuning, the system transitions directly from CSs to MI without exhibiting breathing CSs, highlighting the robustness of stable CSs. The differences in the transition pathways of nonlinear states under different scanning directions reflect the path dependence inherent in the system. This path dependence can be attributed to the coexistence of multiple nonlinear states within overlapping parameter regions, as theoretically illustrated in Fig. 1(a). These findings reveal the significant impact of detuning direction on path selection and provide a solid experimental basis for further exploration of nonlinear state control in coherently driven Kerr fiber ring cavity.

6. Discussion and conclusion

We have systematically observed the transitions among multiple nonlinear states in a Kerr fiber-loop resonator through experiments and numerical simulations. Our experimental results demonstrate a series of nonlinear state transitions by adjusting the pump detuning. These states transition from stable MI to unstable MI, evolves into breathing CSs, and finally stabilize as CSs. The dynamics of various states were recorded by manipulating the pump detuning. These real-time observations demonstrate how to control complex nonlinear phenomena in practical optical systems, paving the way for further research.

To the best of our knowledge, our experimental results show the direct real-time observation of the complete transition from stable MI to stable CS states in a coherently driven Kerr fiber-loop resonator, confirming the formation process of cavity solitons predicted by theory. Additionally, we observed a novel transition from stable CSs directly to unstable MI during decreasing detuning. This observation reveals that the direction of detuning has a significant impact on the nonlinear state transition path. The observed differences in nonlinear state transition pathways under different detuning scan directions highlight the inherent path dependence of the dynamics of a coherently driven Kerr fiber-loop resonator. As shown in the theoretical results presented in Fig. 1(a), multiple nonlinear states coexist within certain parameter regions, indicating that the system can evolve along distinct trajectories depending on how the detuning is varied. The consistency between our experimental observations and numerical simulations demonstrates the predictive power of LLE in capturing complex nonlinear behavior, underscoring the dynamic potential in transitions between nonlinear states. This phenomenon aids pulse shaping and control in ultrafast optical signal processing, improves the frequency stability and bandwidth optimization of optical frequency combs, enhances the speed and reliability of optical communication systems, optimizes the design of nonlinear optical devices, and increases the resolution and accuracy of precision spectroscopy and metrology. By studying this nonlinear state transition process, it is possible to achieve higher performance, precision, and stability in these fields. Finally, in addition to enhancing the understanding of complex spatiotemporal dynamics and transitions between various nonlinear states in coherent Kerr fiber-loop resonators, we anticipate that the results and techniques demonstrated in our work will significantly impact broader research on dissipative systems.

Acknowledgements

Project supported by the National Natural Science Foundation of China (Grant Nos. 12475006 and 12004309) and the Shaanxi Fundamental Science Research Project for Mathematics and Physics (Grant No. 22JSQ036).

References

[1] Sun Y, Parra-Rivas P, Ferraro M, Mangini F and Wabnitz S 2023 *Chaos, Solitons and Fractals* **176** 114064
[2] Erkintalo M, Murdoch S G and Coen S 2022 *J. R. Soc. N. Z.* **52** 149
[3] Leo F, Coen S, Kockaert P, Gorza S P, Emplit P and Haelterman M 2010 *Nat. Photon.* **4** 471
[4] Coulibaly S, Taki M, Bendahmane A, Millot G, Kibler B and Clerc M G 2019 *Phys. Rev. X* **9** 011054
[5] Huang T, Zheng H, Xu G, Pan J, Xiao F, Sun W, Yan K, Chen S, Huang B, Huang Y and Shum P P 2024 *Phys. Rev. A* **109** 013503
[6] Geng J, Xu S, Jin T, Ding S, Yang L, Wang Y and Zhang Y 2024 *Chin. Phys. B* **33** 014208
[7] Dong X, Yang Q, Spiess C, Bucklew V G and Renninger W H 2020 *Phys. Rev. Lett.* **125** 033902

[8] Kippenberg T J, Gaeta A L, Lipson M and Gorodetsky M L 2018 *Science* **361** eaan8083
[9] Jang J K, Erkintalo M, Coen S and Murdoch S G 2015 *Nat. Commun.* **6** 7370
[10] Anderson M, Leo F, Coen S, Erkintalo M and Murdoch S G 2016 *Optica* **3** 1071
[11] Mao D, He Z, Zhang Y, Du Y, Zeng C, Yun L, Luo Z, Li T, Sun Z and Zhao J 2022 *Light Sci. Appl.* **11** 25
[12] Qureshi P C, Ng V, Azeem F, Trainor L S, Schwefel H G L, Coen S, Erkintalo M and Murdoch S G 2022 *Commun. Phys.* **5** 123
[13] Rowley M, Hanzard P H, Cutrona A, Bao H, Chu S T, Little B E, Morandotti R, Moss D J, Oppo G L, Totero Gongora J S, Peccianti M and Pasquazi A 2022 *Nature* **608** 303
[14] Liu X, Yao X and Cui Y 2018 *Phys. Rev. Lett.* **121** 023905
[15] Kang H, Zhou A, Zhang Y, Wu X, Yuan B, Peng J, Finot C, Boscolo S and Zeng H 2024 *Phys. Rev. Lett.* **133** 263801
[16] Wang S, Song B L, Dou X H, Qiao F H, Li X, Wang J B and Lv Z G 2024 *Chin. Phys. Lett.* **41** 074203
[17] Chen L T, Qin L G, Tian L J, Huang J H, Zhou N R and Gong S Q 2024 *Chin. Phys. B* **33** 064204
[18] Guo H, Karpov M, Lucas E, Kordts A, Pfeiffer M H P, Brasch V, Lihachev G, Lobanov V E, Gorodetsky M L and Kippenberg T J 2017 *Nat. Phys.* **13** 94
[19] Xu G, Nielsen A U, Garbin B, Hill L, Oppo G L, Fatome J, Murdoch S G, Coen S and Erkintalo M 2021 *Nat. Commun.* **12** 4023
[20] Wang Y, Anderson M, Coen S, Murdoch S G and Erkintalo M 2018 *Phys. Rev. Lett.* **120** 053902
[21] Zhang H, Du Y, Zeng C, Sun Z, Zhang Y, Zhao J and Mao D 2024 *Sci. Adv.* **10** eadl2125
[22] Wang Y, Garbin B, Leo F, Coen S, Erkintalo M and Murdoch S G 2018 *Opt. Lett.* **43** 3192
[23] Anderson M, Wang Y, Leo F, Coen S, Erkintalo M and Murdoch S G 2017 *Phys. Rev. X* **7** 031031
[24] Godey C, Balakireva I V, Coillet A and Chembo Y K 2014 *Phys. Rev. A* **89** 063814
[25] Leo F, Gelens L, Emplit P, Haelterman M and Coen S 2013 *Opt. Express* **21** 9180
[26] Lugiato L A, Prati F, Gorodetsky M L and Kippenberg T J 2018 *Phil. Trans. Roy. Soc. A: Math. Phys. Eng. Sci.* **376** 20180113
[27] Wu X, Peng J, Boscolo S, Finot C and Zeng H 2023 *Phys. Rev. Lett.* **131** 263802
[28] Peng J, Boscolo S, Zhao Z and Zeng H 2019 *Sci. Adv.* **5** eaax1110
[29] Zakharov V E and Ostrovsky L A 2009 *Physica D* **238** 540
[30] Everitt P J, Sooriyabandara M A, Guasoni M, Wigley P B, Wei C H, McDonald G D, Hardman K S, Manju P, Close J D, Kuhn C C N, Szigeti S S, Kivshar Y S and Robins N P 2017 *Phys. Rev. A* **96** 041601
[31] Kibler B, Fatome J, Finot C, Millot G, Dias F, Genty G, Akhmediev N and Dudley J M 2010 *Nat. Phys.* **6** 790
[32] Solli D R, Ropers C, Koonath P and Jalali B 2007 *Nature* **450** 1054
[33] Dudley J M, Dias F, Erkintalo M and Genty G 2014 *Nat. Photon.* **8** 755
[34] Dudley J M, Genty G, Mussot A, Chabchoub A and Dias F 2019 *Nat. Rev. Phys.* **1** 675
[35] Del'Haye P, Schliesser A, Arcizet O, Wilken T, Holzwarth R and Kippenberg T J 2007 *Nature* **450** 1214
[36] Pasquazi A, Peccianti M, Razzari L, Moss D J, Coen S, Erkintalo M, Chembo Y K, Hansson T, Wabnitz S, Del'Haye P, Xue X, Weiner A M and Morandotti R 2018 *Phys. Rep.* **729** 1
[37] Brasch V, Geiselmann M, Herr T, Lihachev G, Pfeiffer M H P, Gorodetsky M L and Kippenberg T J 2016 *Science* **351** 357
[38] Joshi C, Jang J K, Luke K, Ji X, Miller S A, Klenner A, Okawachi Y, Lipson M and Gaeta A L 2016 *Opt. Lett.* **41** 2565
[39] Liu X, Popa D and Akhmediev N 2019 *Phys. Rev. Lett.* **123** 093901
[40] Herr T, Brasch V, Jost J D, Wang C Y, Kondratiev N M, Gorodetsky M L and Kippenberg T J 2014 *Nat. Photon.* **8** 145
[41] Yi X, Yang Q F, Yang K Y, Suh M G and Vahala K 2015 *Optica* **2** 1078
[42] Mao D, Wang H, Zhang H, Zeng C, Du Y, He Z, Sun Z and Zhao J 2021 *Nat. Commun.* **12** 6712
[43] Bao C, Jaramillo-Villegas J A, Xuan Y, Leaird D E, Qi M and Weiner A M 2016 *Phys. Rev. Lett.* **117** 163901
[44] Yi X, Yang Q F, Yang K Y and Vahala K 2018 *Nat. Commun.* **9** 3565
[45] Li Y, Huang S W, Li B, Liu H, Yang J, Vinod A K, Wang K, Yu M, Kwong D-L, Wang H-T, Wong K K Y and Wong C W 2020 *Light Sci. Appl.* **9** 52
[46] Weng W, Bouchand R and Kippenberg T J 2020 *Phys. Rev. X* **10** 021017
[47] Lugiato L A and Lefever R 1987 *Phys. Rev. Lett.* **58** 2209
[48] Hansson T and Wabnitz S 2015 *J. Opt. Soc. Am. B* **32** 1259
[49] Copie F, Conforti M, Kudlinski A, Mussot A, Biancalana F and Trillo S 2017 *The Eur. Phys. J. D* **71** 133
[50] Coen S and Erkintalo M 2013 *Opt. Lett.* **38** 1790
[51] Yang J and Lakoba T I 2007 *Stud. Appl. Math.* **118** 153